IEEE Access
Multidisciplinary | Rapid Review | Open Access Journal

Received 20 July 2022, accepted 16 August 2022, date of publication 24 August 2022, date of current version 30 August 2022.

Digital Object Identifier 10.1109/ACCESS.2022.3201355

RESEARCH ARTICLE

Quasi Resonant Inverter Load Recognition Method

METIN OZTURK[1,2], FATIH ZUNGOR[2,3], BURHANEDDIN EMRE[2,4], AND BARIS OZ[2,5]

[1]Department of Electrical and Electronics Engineering, Istanbul Esenyurt University, 34510 Istanbul, Turkey
[2]Department of Research and Development, Mamur Technology Systems Inc., 34590 Istanbul, Turkey
[3]Department of Electrical Engineering, Yildiz Technical University, 34220 Istanbul, Turkey
[4]Department of Electrical and Electronics Engineering, Istanbul University, 34320 Istanbul, Turkey
[5]Department of Control and Automation Engineering, Yildiz Technical University, 34220 Istanbul, Turkey

Corresponding author: Metin Ozturk (metinozturk@esenyurt.edu.tr)

This work was supported by the Scientific and Technological Research Council of Turkey Co-Financed by Mamur Technology Systems Research and Developement Center under Project 3210188.

ABSTRACT Induction heating (IH) technology is very popular in domestic applications because of its efficiency and safe operating properties. Resonant inverter circuits are widely used in IH systems owing to their high efficiency and soft-switching capability. Among the resonant inverters used in IH systems, the single-switch quasi-resonant inverter topology is generally preferred for low-cost and low-output-power applications. Despite the low-cost advantage of the quasi-resonant inverter, the soft-switching range is quite narrow, and it is not stable depending on the electrical parameters of the load that is desired to be heated. In other words, there is a critical relationship between the electrical characteristics of the pan, turn-on, and turn-off times, which are the control parameters of the semiconductor switch, and the safe working conditions. In addition, when the importance of closed-loop control methods is evaluated together with the selection of resonant circuit elements, it is essential to determine whether the load is suitable for heating, and to determine the electrical properties of the load to provide both reliable and efficient operating conditions. This study focuses on a new load-detection method based on circuit analysis for quasi-resonant induction hobs. After determining the load parameters, the turn-on and turn-off times of the semiconductor switch were determined to obtain the lowest possible switching loss. Therefore, the boundary conditions of the semiconductor switch are maintained within these limits. The proposed method and its advantages for the switch safe operating area were theoretically examined and proved through simulations and prototype circuits.

INDEX TERMS Home appliances, induction cooking systems, induction cookers, load detection methods, resonant converters, single switch quasi resonant inverter.

I. INTRODUCTION

Induction heating systems are mainly used in industrial, domestic, and medical applications owing to their user safety, efficient heating, easy cleaning, and fast heating features [1], [2], [3]. Domestic induction cooking apparatuses comprise at least one induction coil placed beneath the in vitro ceramic glass surface to heat up pans placed on top of the surface [4], [5], [6], [7], [8], [9]. To heat the pan, the induction coil is supplied with an alternating current that generates a magnetic field at the same frequency as the coil current. This induces eddy currents that cause heating through the pan disposed on the induction surface [4], [6], [10]. The main components of induction heating systems are the rectifier unit, which is used for AC-DC conversion, and resonant inverter units [1], [11], [12]. A general power-transfer loop for domestic appliances is shown in Fig. 1.

Depending on the balance between cost and performance, which must be evaluated for each application, different resonant inverter topologies have been proposed [13], [14].

The associate editor coordinating the review of this manuscript and approving it for publication was Chi-Seng Lam.

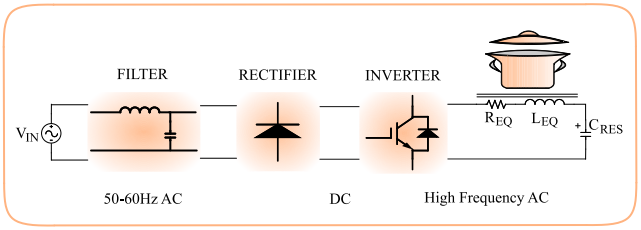

FIGURE 1. General power transfer loop.

The most common inverter topologies in IH systems are half-bridge and single-switch quasi-resonant inverters. The single-switch quasi-resonant inverter topology offers a reliable solution for low-power, low-cost IH applications. The main disadvantage of the quasi-resonant inverter circuit is that it cannot control the power transferred to the load as frequency-controlled, as in half-bridge inverter circuits. The main reason for this is that the working modes of the quasi-resonant inverter switch between *RL* and *RLC* circuits. Therefore, closed-loop control algorithms are used to determine the turn-on and turn-off times of the semiconductor switch.

In IH systems that use quasi-resonant inverters, there is an important relationship among the load parameters, current and voltage limit values of the semiconductor switch, turn-on and turn-off times of the semiconductor switch, and closed-loop power control methods. When the importance of closed-loop power control methods is evaluated together with the selection of resonant circuit elements, it is essential to determine whether the load is suitable for heating and the electrical properties of the load to ensure both reliable and efficient operation conditions. Although common induction heaters are designed to heat ferromagnetic pans, determining the load conditions for every working case is challenging [15], [16], [17]. Because of the relationship between the inverter circuit parameters and the induction loads, load identification methods are critical in induction hob applications, not only for accurate power control but also for reliable design [18], [19], [20], [21], [22], [23], [24], [25], [26], [27].

II. CIRCUIT DESCRIPTION

The circuit diagram and schema of the single-switch quasi-resonant inverter and its main operation waveforms are presented in Fig. 2 and 3, respectively. The circuit schema includes a semiconductor switch T, freewheeling diode D, equivalent resistance R_{EQ}, equivalent inductance L_{EQ} and resonance capacitor C_{RES}. When the switch T is turned on, the circuit acts as a serial *RL* circuit. The coil stores energy through the resistance R_{EQ} for the t_{ON}. The coil stores the energy supplied by the main V_{DC} throughout the turn-on time. When the switch T was turned off, the circuit acted as a serial *RLC* circuit. The coil and capacitor resonate and exchange energy. The resonance capacitor C_{RES} charges the peak voltage V_{CEMAX} and eventually discharges it to zero. The switch was turned on again shortly after the capacitor was fully discharged [28], [29], [30].

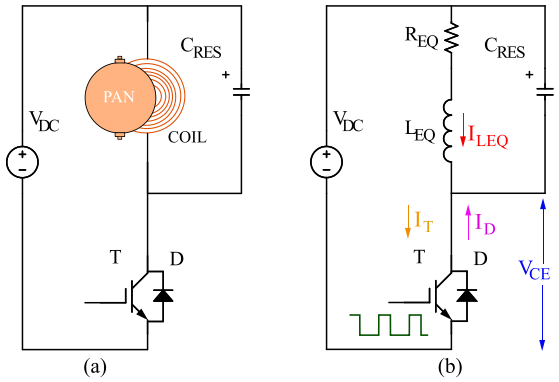

FIGURE 2. Single switch inverter (a) circuit diagram (b) circuit schema.

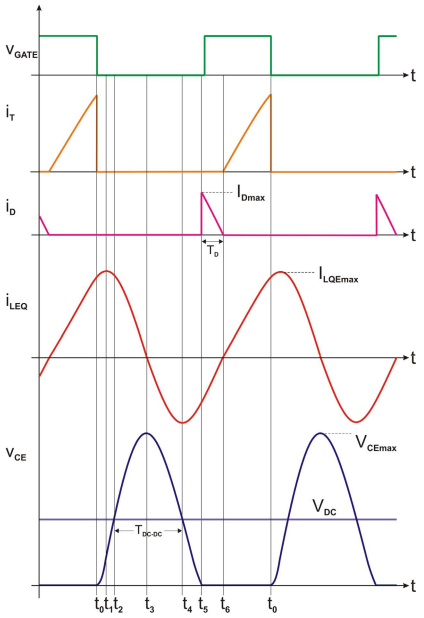

FIGURE 3. Current and voltage waveforms of single switch inverter.

A. CIRCUIT OPERATING MODES – WAVEFORM EQUATIONS

The working modes of the single-switch resonant inverter shown in Fig. 4 were examined in four main operation stages. The conduction time of the T semiconductor $t_6 < t < t_0$ is modeled as a series *RL* circuit that consists of R_{EQ} and L_{EQ}, while the time interval $t_0 < t < t_5$ where resonance occurs between L_{EQ} and C_{RES} is analyzed as a series *RLC* circuit. Finally, the conduction time of the D freewheeling diode $t_5 < t < t_6$ is modeled as a series *RL* circuit. As a result of the single-switch resonant inverter working as a series *RLC* circuit for states 2 and 3 out of 4 operating states and as a series *RL* circuit for operating states 1 and 4, the related circuit is analyzed with the time domain instead of the frequency domain.

Stage I $(t_6 - t_0)$: This interval starts with the T semiconductor's turn-on under zero voltage (ZVT) and continues until the T switch turns off. For the *RL* circuit operation, the

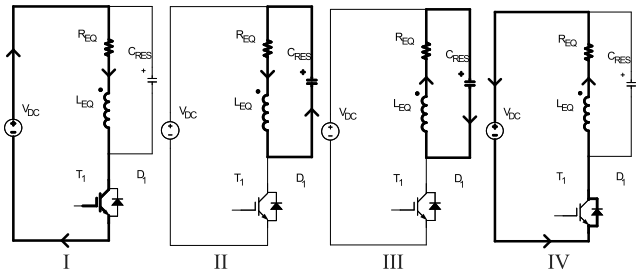

FIGURE 4. Circuit operating modes of single switch inverter.

following equations can be defined as in (1)–(3):

$$i_{LEQ}(t_6) = 0 \tag{1}$$

$$i_{LEQ}(t) = i_T(t) = \frac{V_{DC}}{R_{LEQ}} \cdot (1 - e^{-\frac{R_{EQ}}{L_{EQ}} \cdot t}) \tag{2}$$

$$V_{DC} = V_{LEQ} + V_{REQ} \tag{3}$$

Stage II-III $(t_0 - t_5)$: This interval starts with the turn-off of the T semiconductor, and resonance occurs between L_{EQ} and C_{RES} were analyzed as a series RLC circuit. In addition, the following equations can be defined for I_{LEQ} current, as in (4)–(7).

$$i_{LEQ}(t) = e^{-\alpha t}(B_1 cos(\omega_d t) + B_2 sin(\omega_d t)) \tag{4}$$

$$di_{LEQ}(t)/dt = -e^{-\alpha t}[(B_1\omega_d + B_2\alpha)sin(\omega_d t) + (B_1\alpha - B_2\omega_d)cos(\omega_d t)] \tag{5}$$

$$i_{LEQ}(t_0) \Longrightarrow B_1 = I_0 \tag{6}$$

$$di_{LEQ}(t_0)/dt \Longrightarrow B_2 = ((V_{DC} - R_{EQ}I_0))/(L_{EQ}\omega_d) + (\alpha I_0)/\omega_d \tag{7}$$

In addition, the above equations and circuit equations (8)–(11) can be used to calculate the switch collector-emitter voltage V_{CE} shown in Fig. 3.

$$v(t) = V_{DC} + e^{-\alpha t}(A_1 cos(\omega_d t) + A_2 sin(\omega_d t)) \tag{8}$$

$$dv(t)/dt = -e^{-\alpha t}[(A_1\omega_d + A_2\alpha)sin(\omega_d t) + (A_1\alpha - A_2\omega_d)cos(\omega_d t)] \tag{9}$$

$$v(t_0) \Longrightarrow A_1 = -V_{DC} \tag{10}$$

$$dv(t_0)/dt \Longrightarrow A_2 = (I_0/C_{RES} - \alpha V_{DC})/\omega_d \tag{11}$$

Stage IV $(t_5 - t_6)$: This interval starts with the turning on D diode, which is connected anti-parallel to T power switch. As shown in Fig. 3, the freewheeling of current or energy through the source is handled by a D power diode. For the RL circuit operation, the following equations can be defined as in (12)–(15): The diode current conduction time $t_D(t_6 - t_5)$ and the diode peak current are expressed I_{Dmax}.

$$i_{LEQ}(t) = \frac{V_{DC}}{R_{EQ}} + (I_{Dmax} - \frac{V_{DC}}{R_{EQ}})e^{-\frac{R_{EQ}}{L_{EQ}} \cdot t} \tag{12}$$

$$i_{LEQ}(t_D) = 0 = \frac{V_{DC}}{R_{EQ}} + (I_{Dmax} - \frac{V_{DC}}{R_{EQ}})e^{-\frac{R_{EQ}}{L_{EQ}} \cdot t_D} \tag{13}$$

$$t_D = \ln[\frac{V_{DC}/R_{EQ}}{V_{DC}/R_{EQ} - I_{Dmax}}](-\frac{L_{EQ}}{R_{EQ}}) \tag{14}$$

$$t_D = -\frac{L_{EQ}}{R_{EQ}} \cdot ln\left(1 + \frac{I_{Dmax}}{V_{DC}/R_{EQ} - I_{Dmax}}\right) \tag{15}$$

B. SAFE OPERATING AREA FOR QUASI RESONANT INVERTER

From the first- and second-order circuit equations given above, it is determined that the optimum determination of R_{EQ}, L_{EQ} and C_{RES} values is highly important for safe operating conditions of quasi-resonant induction heating applications. The two main factors that threaten safe working conditions in power electronic circuits are higher voltage and current than the maximum working conditions of the semiconductors used. Although all electronic circuit elements are affected by the overcurrent and overvoltage stresses, semiconductor switches are the most sensitive components in inverter applications. Even if overheating caused by excessive current can be eliminated by forced cooling methods, semiconductors exposed to voltages higher than the breakdown voltage can become inoperable within a very short time. Using the PSpice simulation program, the variances of the semiconductor switch collector-emitter voltage V_{CE} values were obtained for different resonant circuit parameters, as shown in Fig. 5.

In the same manner, C_{RES} capacitor discharge currents, which are frequently observed in quasi-resonant inverter circuits, threaten the reliable operation conditions of both semiconductors and power electronics circuits. These instantaneous currents, also called light load currents, can be three to four times larger than the nominal maximum current of the semiconductor (or coil current I_{LEQ}), and they cause overheating, stress, and similar problems. As in the V_{CE} voltage example, the semiconductor switch current I_T is obtained with the help of the PSpice simulation program, depending on different resonant circuit parameters, as shown in Fig. 6.

However, closed-loop power control techniques and the evaluation of input parameters are important for reliable working conditions. When the quasi-resonant inverter is analyzed, it can be observed that the working modes switch between RL and RLC circuits. Therefore, closed-loop control techniques used to determine the turn-on and turn-off times of semiconductor switches are essential. Depending on the material characteristics, AC supply conditions, and inverter circuit element parameters, calculating the semiconductor switch turn-on or turn-off times with an error greater than $1\mu s$ can rapidly increase switching losses. As a result, the switch is inoperable owing to overheating or overvoltage.

In the next section, a new analysis method is proposed for the identification of the load to be heated.

III. QUASI RESONANT INVERTER ANALYSIS FOR PROPOSED LOAD RECOGNITION METHOD

Similar to other inverter topologies, it is necessary to have knowledge of certain predefined circuit parameters to start the analysis of a quasi-resonant power inverter. By the help

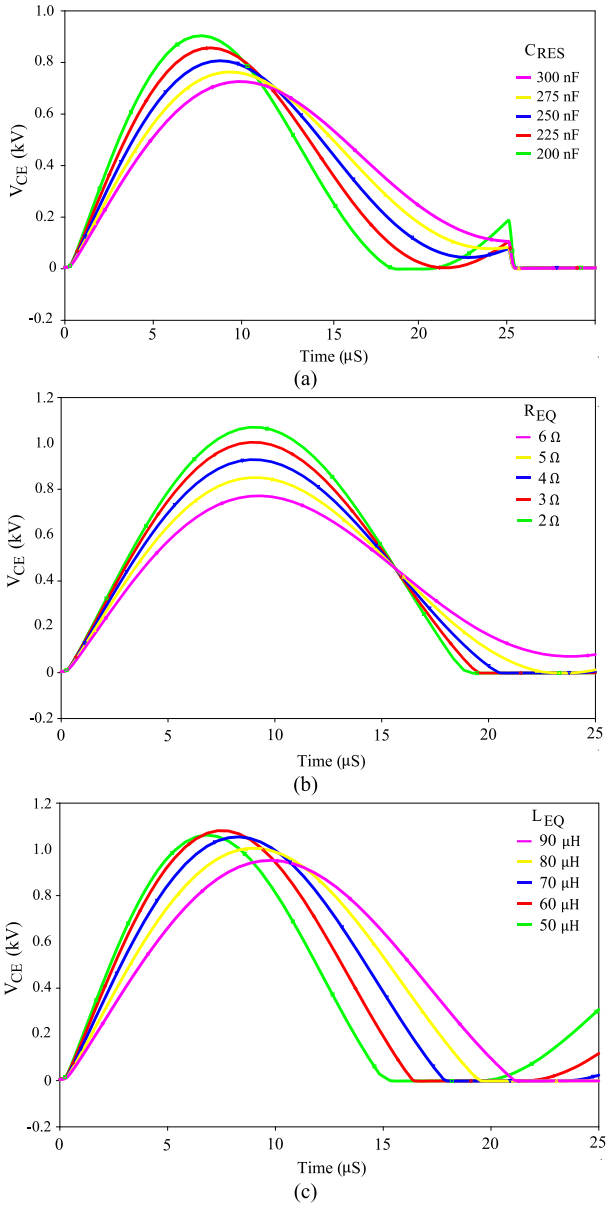

FIGURE 5. V_{CE} **voltage value variances in PSpice. (a)** $R_{EQ} = 3\ \Omega$, $L_{EQ} = 80\ \mu H$ **and depending on** C_{RES} **values. (b)** $C_{RES} = 270$ **nF,** $L_{EQ} = 80\ \mu H$ **and depending on** R_{EQ} **values. (c)** $R_{EQ} = 3\Omega$, $C_{RES} = 270\ nF$ **depending on** L_{EQ} **values.**

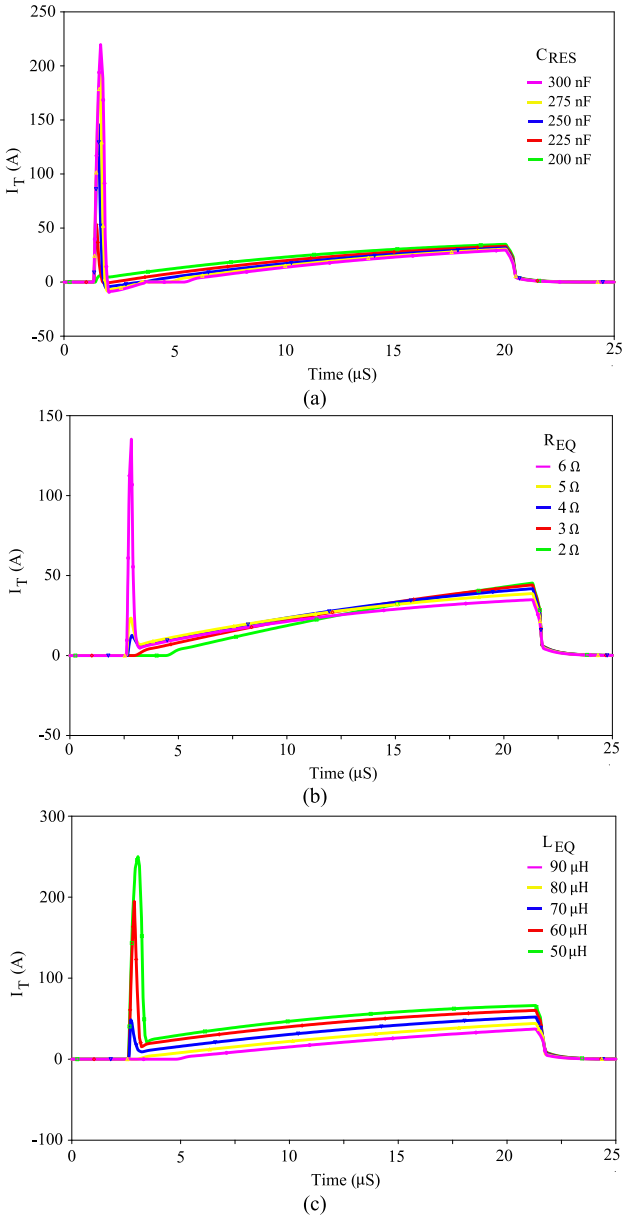

FIGURE 6. I_T **current value variances in PSpice. (a)** $R_{EQ} = 3\ \Omega$, $L_{EQ} = 80\ \mu H$ **and depending on** C_{RES} **values. (b)** $C_{RES} = 270$ **nF,** $L_{EQ} = 80\ \mu H$ **and depending on** R_{EQ} **values. (c)** $R_{EQ} = 3\ \Omega$, $C_{RES} = 270\ nF$ **depending on** L_{EQ} **values.**

of these predefined circuit parameters, and using equations (1)–(54), different inverter analysis methods can be iteratively improved. In this section, a new analysis methodology for calculating the circuit parameters and a new load identification method are proposed. The remainder of this paper is organized as follows.

First, the equations for the time intervals t_0 to t_6 shown in Fig. 3, are defined. Afterwards the damping coefficient α and damped resonant frequency ω_d are obtained from time interval values. Subsequently, the resonant frequency ω_0 is derived from α and ω_d values (50). Then, with the help of ω_0 and C_{RES}, equivalent inductance L_{EQ} is calculated (51). Finally, the equivalent resistance R_{EQ} was calculated using the L_{EQ} and α (52).

A. DEFINING TIME INTERVAL EQUATIONS

In working stages II-III, the coil current I_{LEQ} and switch turn-off voltage V_{CE} reach their maximum values. Knowledge of these two parameters and their boundary conditions is very important and useful for designers not only for reliable working conditions but also for controlling system parameters such as the magnitude of the power transfer to the load. Moreover, the maximum current and voltage values of these quantities are functional in determining the time intervals that are used for the load identification method.

As shown in Fig. 3, when the coil current I_{LEQ} reached its maximum value I_{LEQmax}, the derivation of the I_{LEQ} current

was zero ($t = t_1$). Consequently, the maximum coil current I_{LEQmax} can be derived using (16)–(18).

$$di_{LEQ}(t_1)/dt = 0 \Longrightarrow i_{LEQ}(t_1) = I_{LEQmax} \tag{16}$$

$$t_1 = \tan^{-1}\left[-(B_1\alpha - B_2\omega_d)/(B_1\omega_d + B_2\alpha)\right]/\omega_d \tag{17}$$

$$I_{LEQmax} = i_{LEQ}(t_1) = e^{-\alpha t_1}(B_1 cos(\omega_d t_1) + B_2 sin(\omega_d t_1)) \tag{18}$$

The maximum power level of a single-switch induction cooker is limited by the maximum breakdown voltage level of the power switch. When the switch voltage V_{CE} reaches its maximum value V_{CEmax}, the I_{LEQ} current is zero ($t = t_3$). Consequently, the maximum switch voltage V_{CEmax} can be derived as (19)–(21).

$$i_{LEQ}(t_3) = 0 \Longrightarrow v(t_3) = V_{CEmax} \tag{19}$$

$$t_3 = \tan^{-1}(-B_1/B_2)/\omega_d \tag{20}$$

$$V_{CEmax} = v(t_3) = V_{DC} + e^{-\alpha t_3}(A_1 cos(\omega_d t_3) + A_2 sin(\omega_d t_3)) \tag{21}$$

When serial resonance occurs between L_{EQ} and C_{RES}, the switch voltage V_{CE} passes the DC bus voltage V_{DC} twice (t_2 and t_4). Using (22)–(25), T_{RES} and ω_d can be derived as follows:

$$v(t_2, t_4) = V_{DC} \tag{22}$$

$$v(t_2) = V_{DC} + e^{-\alpha t_2}(A_1 cos(\omega_d t_2) + A_2 sin(\omega_d t_2)) \tag{23}$$

$$t_2 = \tan^{-1}(-A_1/A_2)/\omega_d \tag{24}$$

$$t_4 = t_2 + \pi/\omega_d \tag{25}$$

In addition to the above equations, an approximate approach should be used to calculate t_5. Referring to (8), the following equation is valid for $v(t_5)$.

$$v(t_5) = 0 = V_{DC} + e^{-\alpha t_5}(A_1 cos(\omega_d t_5) + A_2 sin(\omega_d t_5)) \tag{26}$$

Following transformations are applied according to Pythagoras theorem.

$$y_1 = A_1 cos(\omega_d t_5) + A_2 sin(\omega_d t_5) \tag{27}$$

$$A_3 = \sqrt{A_1^2 + A_2^2} \tag{28}$$

According to (27), (28) can be rewritten as following.

$$\frac{y_1}{A_3} = \frac{A_1}{A_3}\cos(\omega_d t_5) + \frac{A_2}{A_3}\sin(\omega_d t_5) \tag{29}$$

where,

$$\frac{A_1}{A_3} = \cos\theta, \frac{A_2}{A_3} = \sin\theta, \theta = atan^2\left(\frac{A_2}{A_1}\right) \tag{30}$$

Equation (45) can be obtained by organizing Equation (29) with the transformations defined in Equation (30).

$$\frac{y_1}{A_3} = \cos\theta\cos(\omega_d t_5) + \sin\theta\sin(\omega_d t_5) \tag{31}$$

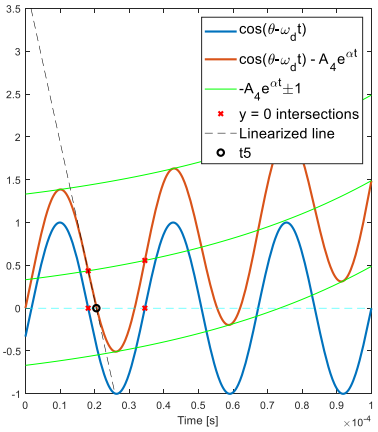

FIGURE 7. Matlab simulation results for t_5 calculation.

Cosine theorem can be used to obtain a compact representation as follows.

$$y_1 = A_3.\cos(\theta - \omega_d t_5) \tag{32}$$

Substituting (32) to (29) ends up with following equation.

$$V_{DC} + e^{-\alpha t_5}.A_3.\cos(\theta - \omega_d t_5) = 0 \tag{33}$$

Following variable is defined to study on frequency analysis.

$$A_4 = -\frac{V_{DC}}{A_3} \tag{34}$$

$$\cos(\theta - \omega_d t_5) = A_4 e^{\alpha t_5} \tag{35}$$

$$f_1(t_5) = \cos(\theta - \omega_d t_5) - A_4 e^{\alpha t_5} \tag{36}$$

The period of $f_1(t_5)$ is exactly equal to the period of $\cos(\theta - \omega_d t_5)$. Owing to the nature of the cosine term, the x-axis intersection points can be defined as follows:

$$x_1 = \frac{1}{\omega_d}\left[\frac{\pi}{2} + \theta\right], \quad x_2 = \frac{1}{\omega_d}\left[\frac{3\pi}{2} + \theta\right] \tag{37}$$

To obtain an appropriate solution, $f_1(t_5)$ is linearized around x_1 point as follows.

$$f_{lin}(t_5) = [t_5 - x_1] \cdot \left.\frac{df_1(t_5)}{dt}\right|_{t_5 = x_1} \tag{38}$$

$$A_5 = \left[\omega_d \sin(\theta - \omega_d x_1) - \alpha A_4 e^{\alpha x_1}\right] \tag{39}$$

$$f_{lin}(t_5) = A_5(t_5 - x_1) \tag{40}$$

The intersection points with the x-axis of $f_{lin}(t_5)$ term can be defined as t_5^* and are derived as follows:

$$t_5^* = x_1 - \frac{1}{A_5} f_1(x_1) \tag{41}$$

$$t_5^* = \frac{1}{\omega_d}\left[\frac{\pi}{2} + \theta\right] + \frac{A_4}{A_5} e^{\frac{\alpha}{\omega_d}\left[\frac{\pi}{2} + \theta\right]} \tag{42}$$

Because the descending edge of $f_1(t_5)$ is sharp, an approximate solution of t_5^* is appropriate to satisfy the design requirements. Fig. 7 shows the approximate t_5^* calculation. For the proposed method, it was appropriate to assume $t_5 = t_5^*$.

Then, using (4) and (42), the diode current peak value I_{Dmax} and diode conduction time interval t_D can be determined, respectively.

$$I_{Dmax} = i_{LEQ}(t_5) = e^{-\alpha t_5}(B_1 cos(\omega_d t_5) + B_2 sin(\omega_d t_5)) \quad (43)$$

$$t_D = -\frac{L_{EQ}}{R_{EQ}} \cdot ln\left(1 + \frac{I_{Dmax}}{V_{DC}/R_{EQ} - I_{Dmax}}\right) \quad (44)$$

$$t_D = t_6 - t_5 \quad (45)$$

B. DEFINING RLC CIRCUIT PARAMETERS

α, ω_d and ω_0 The time intervals obtained from circuit operation modes such as t_2, t_3 and t_4 can be determined using digital measurement methods. For this purpose, it is useful and practical to use microcontrollers or similar digital circuit components. In addition, provided that the resonant capacitor C_{RES} is known, the unknown circuit parameters can be calculated using Equations (49)–(52).

The resonant period T_{RES} value can be found using with t_2 and t_4 time intervals.

$$T_{RES} = 2.(t_4 - t_2) = 2.\pi/\omega_d \quad (46)$$

By the help of the equation (46), the damped resonant frequency ω_d value is obtained from t_2 and t_4 time intervals (47).

$$\omega_d = 2\pi/(2.(t_4 - t_2)) \quad (47)$$

Through the rearrangement of equations (4) and (5) and equation (48), the damping coefficient α is found.

$$\alpha = \omega_d.\cot(\omega_d.(t_1 - t_3)) \quad (48)$$

It is not easy to measure the t_1 time intervals practically. Fortunately, from the circuit equations mentioned previously, it is clear that the t_1 value can be obtained from the t_3 and the t_4 time intervals.

$$t_1 = 2t_3 - t_4 \quad (49)$$

Alpha can also be found using the following equations: One of these equations can be selected according to the controller abilities.

$$\alpha = \omega_d.\cot(\omega_d.(t_3 - t_4))$$
$$\alpha = \omega_d.\cot(\omega_d.(t_3 - t_2))$$

For the serial *RLC* circuit, α and ω_d values are very beneficial for finding unknown circuit parameters, such as equivalent resistance R_{EQ} and equivalent inductance L_{EQ}. The resonant frequency ω_0 is derived from α and ω_d values (50).

$$\omega_d = \sqrt{\omega_0^2 - \alpha^2} \quad (dampedres.frequency) \quad (50)$$

The equivalent inductance L_{EQ} is calculated by using ω_0 and C_{RES}.

$$\omega_0 = 1/\sqrt{L_{EQ}C_{RES}} \quad (resonant\ frequency) \quad (51)$$

And the equivalent resistance R_{EQ} is calculated with using the L_{EQ} and α (52).

$$\alpha = R_{EQ}/2L_{EQ}(damping\ coefficient) \quad (52)$$

Finally, $t_6 - t_o$ time interval can be found by the help of (2).

$$I_0 = i_{LEQ}(t_6 - t_o) = \frac{V_{DC}}{R_{EQ}}\left(1 - e^{-\frac{R_{EQ}}{L_{EQ}}\cdot(t_6 - t_0)}\right) \quad (53)$$

$$t_6 - t_o = -\frac{L_{EQ}}{R_{EQ}} \cdot ln\left(1 - \frac{I_0}{V_{DC}/R_{EQ}}\right) \quad (54)$$

IV. PROPOSED LOAD RECOGNITION METHOD

After analyzing the time intervals of the quasi-resonant inverter operation, a new load recognition method is proposed using the relevant time intervals, which are the outputs of the analysis studies. In the proposed method, t_2, t_3 and t_4 time intervals were considered sufficient for the load recognition method. However, considering that the time intervals obtained with the help of the analyses in the first chapter will shed light on different studies on the subject, all the equations obtained in the study are preserved.

In quasi-resonant inverter circuits used in domestic induction heating hobs, the determination of the turn-on and turn-off times of the semiconductor switch is important for operation under soft-switching conditions. Because the load to be heated is variable and unknown, the electrical parameters of the load should first be determined correctly, and then the turn-on and turn-off times suitable for these characteristics should be determined. For this purpose, a small amount of energy is transferred to the coil by turning the semiconductor switch on so that the inverter circuit can operate safely and the time intervals required by the proposed method can be determined. In practice, the initial turn-on time of the switch is of the order of $2\mu s$. Depending on the resonance that will occur between the coil and capacitor, the time intervals t_2, t_3 and t_4 are measured. The electrical parameters of the load to be heated were determined using the proposed analytical method. Finally, with the help of the proposed analysis method, the turn-on and turn-off times (t_{ON} and t_{OFF}) of the switch are determined, and operation under soft-switching conditions is ensured.

The visual algorithm, shown in Fig. 8, was developed to understand the process more clearly. At the end of the process, which starts with the input pulse signal, both load parameters are determined, and the semiconductor switch turn-on and turn-off times that provide the soft switching positions are determined.

The quasi-resonant inverter analysis method, which is analyzed in detail in this section, is verified by simulation and induction hob implementation in the next section. Although the proposed analysis method to determine the equivalent resistance R_{EQ} and equivalent inductance L_{EQ} with the help of the time intervals is very useful for practical implementation, the accurate determination of α and ω_d is very important.

V. VERIFICATION OF PROPOSED LOAD RECOGNITION METHOD

The results obtained from the analysis are confirmed by simulation and application studies in this section. After the completion of the theoretical background studies developed for

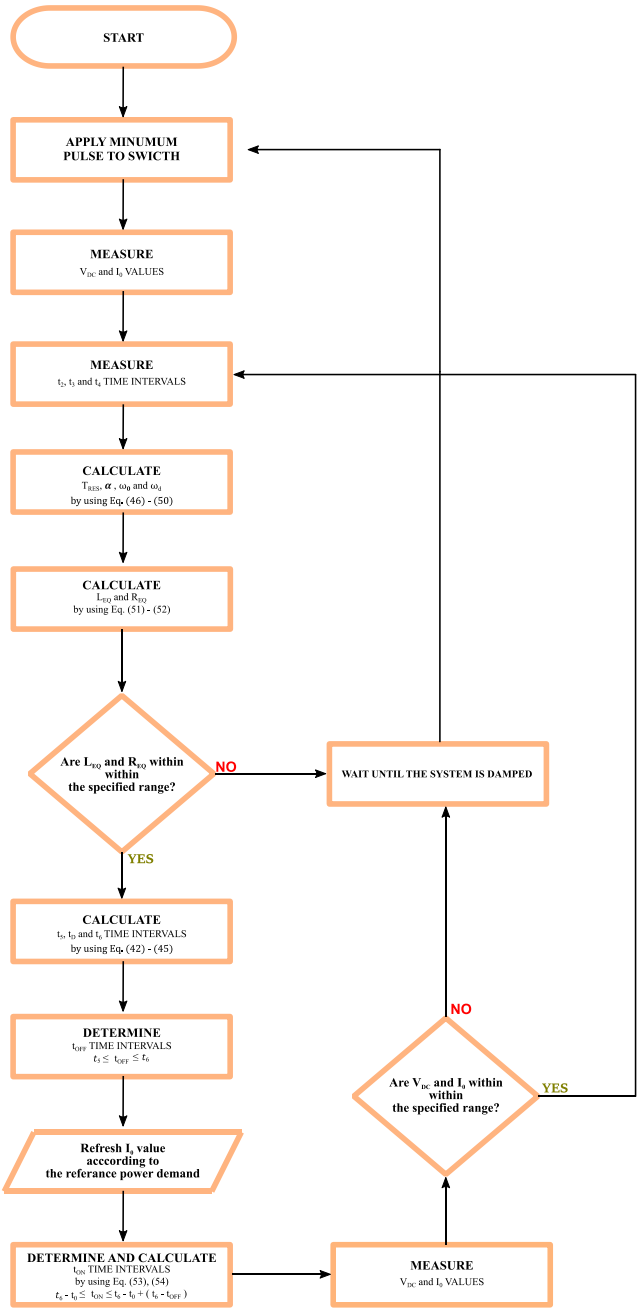

FIGURE 8. The visual algorithm of determining circuit control parameters.

use in load identification studies, the outputs of the relevant analysis methods were first run in the simulation environment and then applied with the help of a practical application circuit.

To make an accurate comparison, four different ferromagnetic pans were used as loads in the simulation and experimental studies. When Table 1 is examined in detail, it can be observed that each pan has different ferromagnetic characteristics. The pans used were selected from different points in the ferromagnetic spectrum. Thus, we attempted to prove that the proposed method is suitable for all pans

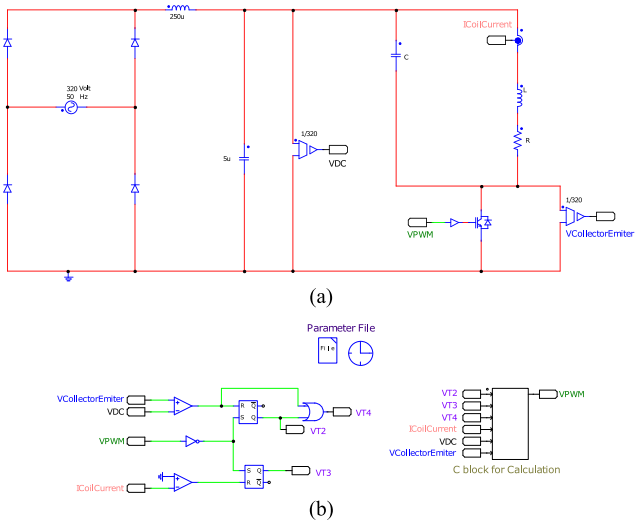

FIGURE 9. PSIM Simulation Circuit Applications. (a) General quasi-resonant circuit. (b) Logic circuits for obtaining t_2,t_3 and t_4 time intervals.

used in practice. The values obtained from the simulation and application were compared, and the reliability of the analysis was proved.

A. SIMULATION RESULTS

The simulation circuit application achieved using the PSIM program is shown in Fig. 9-a. It includes the AC main source, induction hob resonant tank, related current and voltage measurement tools, and a circuit parameter calculator. As shown in Fig. 9-b, the logic gates and flip-flop circuits are used to determine the t_2, t_3 and t_4 time intervals. As described above section, time intervals are used as input values to calculate other circuit parameters such as α, ω_0, R_{EQ} and L_{EQ}. As an output of this simulation circuit, V_{Gate} is the semiconductor switch gate voltage, V_{DC} is the DC bus voltage, V_{CE}

B. EXPERIMENTAL VERIFICATIONS

The circuit scheme of the induction cooktop with quasi-resonant topology is shown in Fig. 11. The experimental circuit prototype is shown in Fig. 12. The main supply voltage $V_{AC} = 230$ VAC and rectified DC bus voltage $V_{DC} = 320$V. A GSIB2560 bridge rectifier was used in the rectifier circuit. Because the IHW20N135R5 IGBT with the body diode is used as a switch, an additional diode is not used in the circuit and $C_{RES} = 270$ nF. An advanced ARM-based 32-bit MCU STM32F100R8 microprocessor is used in the prototype application circuit. The operating frequency of the processor was $16MHz$. The I_{LEQ} coil current readings were made using a $10m\Omega$ shunt resistor and an op-amp circuit. The switch turn-off voltage, I_{LEQ} coil current, and defined time interval values are shown in Fig. 10.

Voltage readings are obtained with the help of the voltage divider resistor circuit and the ADC channel of the processor. The coil current and switch voltages are read in multiples of $10ms$ and placed in the array, the highest and lowest values are

TABLE 1. Si mulation and experimental results for R_{EQ} and L_{EQ}.

Pan Type	Simulated Results		Experimental Results		Measument Results obtanied from LCR Meter at 20kHz	
	R_{EQ}	L_{EQ}	R_{EQ}	L_{EQ}	R_{EQ}	L_{EQ}
Stainless Steel 12cm	3,06Ω	89,97μH	2,4Ω	92,70μH	3,05Ω	92,65μH
Silargan	1,11Ω	70,76μH	2,4Ω	74,75μH	1,28Ω	74,75μH
Stainless Steel 18cm	2,99Ω	85,30μH	4,83Ω	86,24μH	3,96Ω	88,85μH
Iron	5,29Ω	89,04μH	5,3Ω	94,74μH	4,96Ω	95,24μH

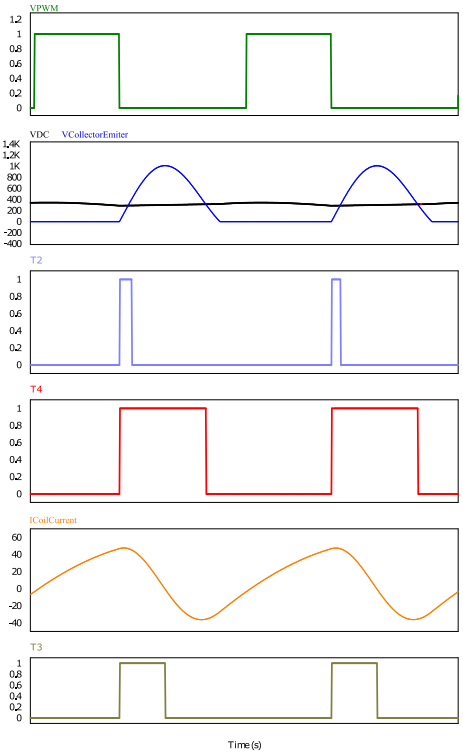

FIGURE 10. PSIM simulation circuit application results.

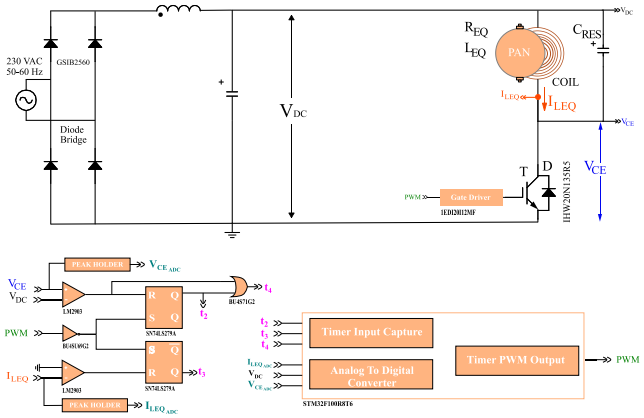

FIGURE 11. The experimental circuit implementation.

FIGURE 12. Experimental prototype.

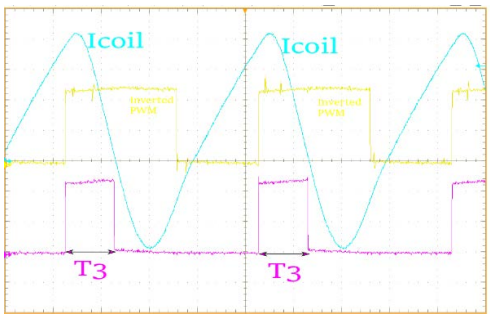

FIGURE 13. Blue signal: I_{LEQ} coil current (20A/div), purple signal: t_3 time interval value (1V/div), yellow signal: inverse of V_{GE} gate voltage (5V/div).

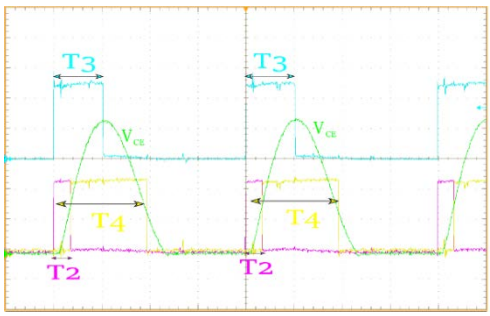

FIGURE 14. Blue signal: t_3 time interval value (1V/div), purple signal: t_2 time interval value (1V/div), yellow signal: t_4 time interval value (1V/div), and green signal: V_{CE} switch voltage value (200V/div).

eliminated, and the average value of eight current and voltage data is used. The experimental prototype circuit results are shown in Fig. 13 and 14. The results were measured using simulations, and the prototype circuits are compared in Table 1 for four different ferromagnetic pans. When a visual algorithm is used to determine the L_{EQ} and R_{EQ} load parameters, the quadratic circuit parameters are determined. Afterwards the load parameters L_{EQ} and R_{EQ} are found with

TABLE 2. Si mulation and experimental results for I_{LEQMAX} and V_{CEMAX}.

Pan Type	Simulated Results		Experimental Results		Differences Between Simulated and Experimental Results	
	I_{LEQMAX}	V_{CEMAX}	I_{LEQMAX}	V_{CEMAX}	% I_{LEQMAX}	% V_{CEMAX}
Stainless Steel 12cm	40,12 A	939,75 V	40,27 A	976,38 V	% 0,3	% 3,7
Silargan	41,74 A	950,18 V	40,83 A	902,79 V	% 2,2	% 4,9
Stainless Steel 18cm	40,29 A	925,59 V	39,61 A	861,18 V	% 1,7	% 6,9
Cast Iron	39,73 A	930,71 V	39,28 A	877,03 V	% 1,1	% 5,7

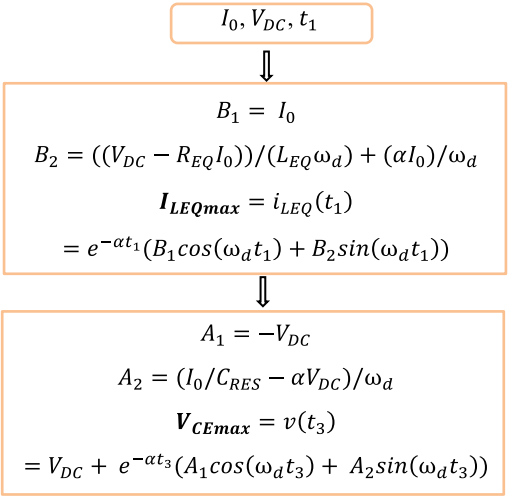

FIGURE 15. Green signal: V_{CE} switch voltage value (200V/div). Visual algorithm for determining I_{LEQmax} and V_{CEmax}.

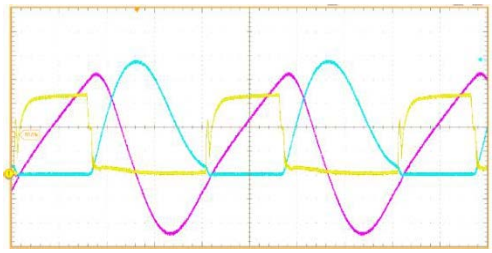

FIGURE 16. Stainless Steel pan circuit waveforms. Blue signal: IGBT collector emitter voltage V_{CE} (200V/div), purple signal: coil current I_{LEQ} (10A/div), yellow signal: IGBT gate control signal (5V/div).

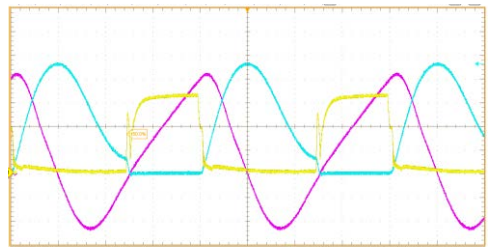

FIGURE 17. Cast iron pan-circuit waveforms. Blue signal: IGBT collector emitter voltage V_{CE} (200V/div), purple signal: coil current I_{LEQ} (10A/div), yellow signal: IGBT gate control signal (5V/div).

the help of the obtained circuit parameters. The same method is valid in both simulation and experimental studies. However, we cannot easily provide these details in the simulation and experimental result tables. Therefore, we directly obtained the final load parameter results. As a result, when the differences between the simulation and experimental results were examined, the equivalent inductance deviation was less than %6. Although the equivalent resistance deviation was not as low as the equivalent inductance, the comparison results were sufficient for the proposed load identification method.

C. BOUNDARY CONDITION ANALYSIS

Despite the benefits of the quasi-resonant inverter, there is a critical relationship between the load parameters and the current and voltage limits of the semiconductor switch. After defining the load parameters using the proposed method, the simulation and experimental results are compared in terms of the boundary condition. As a result of obtaining L_{EQ} and R_{EQ} values using the proposed analysis method, semiconductor switch boundary conditions were also analyzed. The coil current I_{LEQ} and switch turn-off voltage V_{CE} are very important and useful for the designer not only for reliable working conditions, but also for controlling system parameters such as the magnitude of the power transfer to the load. The visual algorithm developed to determine the I_{LEQmax} and V_{CEmax} values is shown in Fig. 15. While determining the circuit parameters with the help of the proposed method, the relevant time intervals and other circuit parameters were first determined. When the proposed method is used, the circuit is maintained within safe operating limits, and a satisfactory difference is measured between the simulation and application results. For this purpose, simulation and application results are presented. For this purpose, a comparative study was conducted for the safe operating limits listed in Table 2. The boundary conditions obtained with the boundary conditions obtained with the help of the measured results from the simulation and prototype circuits are compared in Table 2 for four different ferromagnetic pans. When the differences between the simulation and experimental results were examined, it was observed that the

maximum semiconductor current deviation was $<\%3$ and the maximum semiconductor collector voltage deviation is less than %7. Similar to previous results, the comparison results were sufficient for the proposed load identification method.

Some experimental results are shown in Fig. 16 for the stainless-steel pan and in Fig. 17 for the iron pan. When the experimental results were examined, it was observed that the quasi-resonant inverter remained in the safe operating area when the load detection parameters obtained using the proposed method were used.

VI. CONCLUSION

The proposed method focuses on a new load detection method based on circuit analysis for quasi-resonant induction hobs. The time intervals obtained from circuit operation modes such as t_2, t_3 and t_4 can be determined using digital measurement methods. As a result of obtaining L_{EQ} and R_{EQ} values with the help of the proposed analysis method, the turn-on and turn-off times of the semiconductor switch, as well as the boundary conditions, are analyzed. For this purpose, it is useful and practical to use microcontrollers or similar digital circuit components. In addition, if the resonant capacitor C_{RES} is known, unknown circuit parameters can be calculated. Although the proposed analysis method to determine the equivalent resistance R_{EQ} and equivalent inductance L_{EQ} with the help of time intervals is very useful for practical applications, the accurate determination of α and ω_d is very important.

After the completion of the theoretical background studies developed for use in load identification studies, the outputs of the relevant analysis methods were first run in the simulation environment and then applied with the help of a practical application circuit. The results measured from the simulation and the prototype circuits are compared in terms of circuit parameters, such as the equivalent resistor, inductor, and boundary conditions for four different ferromagnetic pans. The values obtained from the simulation and application were compared, and the reliability of the analysis was proved.

REFERENCES

[1] H. Sarnago, O. Lucia, A. Mediano, and J. M. Burdio, "A class-E direct AC–AC converter with multicycle modulation for induction heating systems," *IEEE Trans. Ind. Electron.*, vol. 61, no. 5, pp. 2521–2530, May 2014, doi: 10.1109/TIE.2013.2281164.

[2] S. Shibuya, W. Kitagawa, and T. Takeshita, "Control of switching frequency twice the output frequency for a matrix converter in induction heating application," in *Proc. 9th Int. Conf. Renew. Energy Res. Appl. (ICRERA)*, Sep. 2020, pp. 227–231, doi: 10.1109/ICRERA49962.2020.9242824.

[3] H. Ishida, K. Nakao, N. Nakao, and N. Kimura, "Efficient heating of mixer by induction heating of mixing blade and energy transfer analysis for optimization," in *Proc. IEEE 6th Int. Conf. Renew. Energy Res. Appl. (ICRERA)*, Nov. 2017, pp. 321–326, doi: 10.1109/ICRERA.2017.8191287.

[4] H. Omori and M. Nakaoka, "New single-ended resonant inverter circuit and system for induction-heating cooking apparatus," *Int. J. Electron.*, vol. 67, no. 2, pp. 277–296, Aug. 1989, doi: 10.1080/00207218908921081.

[5] S. Llorente, F. Monterde, J. M. Burdio, and J. Acero, "A comparative study of resonant inverter topologies used in induction cookers," in *Proc. 17th Annu. IEEE Appl. Power Electron. Conf. Expo.*, vol. 2, Mar. 2002, pp. 1168–1174, doi: 10.1109/APEC.2002.989392.

[6] V. Crisafulli and C. V. Pastore, "New control method to increase power regulation in a AC/AC quasi resonant converter for high efficiency induction cooker," in *Proc. 3rd IEEE Int. Symp. Power Electron. Distrib. Gener. Syst. (PEDG)*, Jun. 2012, pp. 628–635, doi: 10.1109/PEDG.2012.6254068.

[7] L. Meng, K. W. E. Cheng, and K. W. Chan, "Systematic approach to high-power and energy-efficient industrial induction cooker system: Circuit design, control strategy, and prototype evaluation," *IEEE Trans. Power Electron.*, vol. 26, no. 12, pp. 3754–3765, Dec. 2011.

[8] J. Acero, C. Carretero, Ó. Lucía, R. Alonso, and J. M. Burdío, "Mutual impedance of small ring-type coils for multiwinding induction heating appliances," *IEEE Trans. Power Electron.*, vol. 28, no. 2, pp. 1025–1035, Feb. 2013, doi: 10.1109/TPEL.2012.2205270.

[9] S. Okudaira and K. Matsuse, "Adjustable frequency quasi-resonant InverterCircuits having short-circuit SwitchAcross resonant capacitor," *IEEE Trans. Power Electron.*, vol. 23, no. 4, pp. 1830–1838, Jul. 2008, doi: 10.1109/TPEL.2008.924838.

[10] A. Beato, C. Bocchiola, and S. Frattesi, "Modelling and design of the half-bridge resonant inverter for induction cooking application," in *Proc. 14th Medit. Conf. Control Autom.*, Jun. 2006, pp. 4–9, doi: 10.1109/MED.2006.328704.

[11] H. Sarnago, O. Lucia, A. Mediano, and J. M. Burdio, "Direct AC–AC resonant boost converter for efficient domestic induction heating applications," *IEEE Trans. Power Electron.*, vol. 29, no. 3, pp. 1128–1139, Mar. 2014, doi: 10.1109/TPEL.2013.2262154.

[12] A. Sular, A. Mamizadeh, N. Genc, and M. Karaca, "PV power based duty cycle control of quasi-resonant inverter for induction cooking," in *Proc. 8th Int. Conf. Renew. Energy Res. Appl. (ICRERA)*, Nov. 2019, pp. 804–809, doi: 10.1109/ICRERA47325.2019.8996565.

[13] H. Sarnago, O. Lucia, A. Mediano, and J. M. Burdio, "Efficient and cost-effective ZCS direct AC–AC resonant converter for induction heating," *IEEE Trans. Ind. Electron.*, vol. 61, no. 5, pp. 2546–2555, May 2014, doi: 10.1109/TIE.2013.2262752.

[14] M. Ozturk, S. Aslan, N. Altintas, and S. Sinirlioglu, "Comparison of induction cooker power converters," in *Proc. 6th Int. Conf. Control Eng. Inf. Technol. (CEIT)*, Oct. 2018, pp. 1–6, doi: 10.1109/CEIT.2018.8751920.

[15] J. Acero, I. Lope, C. Carretero, and J. M. Burdio, "Adapting of non-metallic cookware for induction heating technology via thin-layer non-magnetic conductive coatings," *IEEE Access*, vol. 8, pp. 11219–11227, 2020, doi: 10.1109/ACCESS.2020.2965209.

[16] J. Acero, I. Lope, C. Carretero, and J. M. Burdio, "Analysis and modeling of the forces exerted on the cookware in induction heating applications," *IEEE Access*, vol. 8, pp. 131178–131187, 2020, doi: 10.1109/ACCESS.2020.3009754.

[17] M. S. Huang, C. C. Liao, Z. F. Li, Z. R. Shih, and H. W. Hsueh, "Quantitative design and implementation of an induction cooker for a copper pan," *IEEE Access*, vol. 9, pp. 5105–5118, 2021, doi: 10.1109/ACCESS.2020.3046713.

[18] O. Lucia, D. Navarro, P. Guillen, H. Sarnago, and S. Lucia, "Deep learning-based magnetic coupling detection for advanced induction heating appliances," *IEEE Access*, vol. 7, pp. 181668–181677, 2019, doi: 10.1109/ACCESS.2019.2960109.

[19] J. Acero, C. Carretero, I. Millán, Ó. Lucía, R. Alonso, and J. M. Burdío, "Analysis and modeling of planar concentric windings forming adaptable-diameter burners for induction heating appliances," *IEEE Trans. Power Electron.*, vol. 26, no. 5, pp. 1546–1558, May 2011, doi: 10.1109/TPEL.2010.2085453.

[20] A. Bono-Nuez, B. Martin-del-Brio, C. Bernal-Ruiz, F. J. Perez-Cebolla, A. Martinez-Iturbe, and I. Sanz-Gorrachategui, "The inductor as a smart sensor for material identification in domestic induction cooking," *IEEE Sensors J.*, vol. 18, no. 6, pp. 2462–2470, Mar. 2018, doi: 10.1109/JSEN.2018.2795739.

[21] J. Villa, L. A. Barragan, J. I. Artigas, D. Navarro, A. Dominguez, and T. Cabeza, "SoC-based in-cycle load identification of induction heating appliances," *IEEE Trans. Ind. Electron.*, vol. 68, no. 8, pp. 6762–6772, Aug. 2021, doi: 10.1109/TIE.2020.3007083.

[22] J. Villa, D. Navarro, A. Dominguez, J. I. Artigas, and L. A. Barragan, "Vessel recognition in induction heating appliances—A deep-learning approach," *IEEE Access*, vol. 9, pp. 16053–16061, 2021, doi: 10.1109/ACCESS.2021.3052864.

[23] J. Acero, C. Carretero, R. Alonso, and J. M. Burdio, "Quantitative evaluation of induction efficiency in domestic induction heating applications," *IEEE Trans. Magn.*, vol. 49, no. 4, pp. 1382–1389, Apr. 2013.

[24] O. Jimenez, O. Lucia, I. Urriza, L. A. Barragan, and D. Navarro, "Analysis and implementation of FPGA-based online parametric identification algorithms for resonant power converters," *IEEE Trans. Ind. Informat.*, vol. 10, no. 2, pp. 1144–1153, May 2014.
[25] A. Dominguez, A. Otin, I. Urriza, L. A. Barragan, D. Navarro, and J. I. Artigas, "Load identification of domestic induction heating based on particle swarm optimization," in *Proc. IEEE 15th Workshop Control Modeling Power Electron. (COMPEL)*, Jun. 2014, pp. 1–6.
[26] M. Ozturk, U. Oktay, N. Yilmaz, H. S. Yardibi, and S. Sinirlioglu, "Comparison of pan detection methods for single switch topology used in domestic induction cooking," in *Proc. Int. Conf. Smart Energy Syst. Technol. (SEST)*, Sep. 2020, pp. 1–6, doi: 10.1109/SEST48500.2020.9203253.
[27] F. Zungor, B. Emre, B. Oz, and M. Ozturk, "A new load detection method and circuit analysis for quasi resonant inverter," in *Proc. 10th Int. Conf. Renew. Energy Res. Appl. (ICRERA)*, Sep. 2021, pp. 40–46, doi: 10.1109/ICRERA52334.2021.9598568.
[28] H. Terai, I. Hirota, T. Miyauchi, H. Omori, K. Ogura, Y. Hirota, and M. Nakaoka, "Comparative performance evaluations of IGBTs and MCT in single-ended quasi-resonant zero voltage soft switching inverter," in *Proc. IEEE 32nd Annu. Power Electron. Spec. Conf.*, Jun. 2001, pp. 2178–2182.
[29] H. Omori, H. Yamashita, M. Nakaoka, and T. Maruhashi, "A novel type induction-heating single-ended resonant inverter using new bipolar darlington-transistor," in *Proc. IEEE Power Electron. Spec. Conf.*, Jun. 1985, pp. 590–599, doi: 10.1109/PESC.1985.7070998.
[30] W. P. W. Komatsu, "A simple and reliable class e inverter for induction heating applications," *Int. J. Electron.*, vol. 84, no. 2, pp. 157–165, Feb. 1998, doi: 10.1080/002072198134922.

METIN OZTURK was born in Kastamonu, Turkey, in 1981. He received the B.S., M.S., and Ph.D. degrees in electrical engineering from Yildiz Technical University, Istanbul, Turkey, in 2004, 2007, and 2018, respectively.

From 2006 to 2016, he was an Electrical Engineer with the Research and Development Department, Arçelik Inc. Since 2016, he has been an Electrical Engineer with the Research and Development Department, Mamur Technology Inc. Since 2018, he has been an Assistant Professor at Istanbul Esenyurt University. His research interests include the domestic induction cooking and development of half bridge and quasi resonant inverter in induction heating.

FATIH ZUNGOR was born in Istanbul, Turkey, in 1994. He received the B.S. degree in electrical and electronic engineering from Sakarya University, Sakarya, Turkey, in 2016, and the M.S. degree in electrical engineering from Yildiz Technical University, Istanbul, in 2018, where he is currently pursuing the Ph.D. degree. From 2016 to 2018, he was a Research and Development Engineer with the Research and Development Department, Gedik Welding. Since 2018, he has been working as a Research and Development Engineer with the Research and Development Department, Mamur Technology. He has authored or coauthored three conference papers in the area of power electronics. He also engaged in three research projects involving power electronics. His current research interests include power factor correction, switching power supplies, high-frequency power conversion, induction heating, and active and passive snubber cells in power electronics.

BURHANEDDIN EMRE was born in Malatya, Turkey, in 1994. He received the B.S. degree in electrical and electronics engineering from Istanbul University, Istanbul, Turkey, in 2019, where he is currently pursuing the M.S. degree in electrical and electronics engineering.

Since 2020, he has been an Electronics Engineer at the Research and Development Department, Mamur Technology Inc. His current research interests include power supply switching, high-frequency power conversion, and induction heating.

BARIS OZ was born in Istanbul, Turkey, in 1988. He received the B.Sc. degree in electrical engineering from Yildiz Technical University, and the M.Sc. degree in mechanical engineering from Istanbul Technical University. He is currently pursuing the Ph.D. degree in control and automation engineering with Yildiz Technical University. He has been working with the Research and Development Center, Mamur Technology Inc., as a Research and Development Project Manager. His current research interests include control systems, machine vision, industrial image-processing applications, optimization, and dynamical system modeling.